η collective mode as A_{1g} Raman resonance in cuprate superconductors

X. Montiel,[*] T. Kloss,[†] and C. Pépin[‡]

Institut de Physique Théorique, CEA-Saclay, 91191 Gif-sur-Yvette, France

S. Benhabib, Y. Gallais, and A. Sacuto

Laboratoire Matériaux et Phénomènes Quantiques (UMR 7162 CNRS), Université Paris Diderot-Paris 7, Bâtiment Condorcet,
75205 Paris Cedex 13, France

We discuss the possible existence of a spin singlet excitation with charge ± 2 (η mode) originating the A_{1g} Raman resonance in cuprate superconductors. This η mode relates the d-wave superconducting singlet pairing channel to a d-wave charge channel. We show that the η boson forms a particle-particle bound state below the 2Δ threshold of the particle-hole continuum where Δ is the maximum d-wave gap. Within a generalized random phase approximation and Bethe-Salpeter approximation study, we find that this mode has energies similar to the resonance observed with inelastic neutron scattering below the superconducting (SC) coherent peak at 2Δ in various SC cuprate compounds. We show that it is a very good candidate for the resonance observed in Raman scattering below the 2Δ peak in the A_{1g} symmetry. Since the η mode sits in the $S = 0$ channel, it may be observable via Raman, x-ray, or electron energy loss spectroscopy probes.

I. INTRODUCTION

The study of collective excitations of a condensed matter system can provide information about the symmetries of an order parameter or the nature of the interactions between particles. The analysis of collective modes can also help us to understand the origin of high critical temperature superconductivity (SC) in cuprate compounds (see schematic cuprate compound phase diagram in Fig. 1).

The existence of a collective spin excitation in the SC state of cuprates has been highlighted by inelastic neutron scattering (INS) experiments with the observation of a resonance at 41 meV in YBCO compounds and at similar energies in other compounds [1–3] around the antiferromagnetic (AF) ordering vector $\mathbf{Q} = (\pi,\pi)$. This resonance, which stands below the $2\Delta_{SC}^0$ threshold of the particle-hole continuum (Δ_{SC}^0 is the maximum of the d-wave SC gap), seems to scale with the superconducting gap energy above optimal doping (at least until $p = 0.19$ hole doping in Bi2212) [4].

This INS resonance has initially been explained in the framework of the SO(5) emergent symmetry model for cuprates as a π mode [5,6]. However this π mode lies at higher energies than experimentally observed, and the neutron resonance is now explained as a spin triplet exciton or resonance which emerges in the SC state because of a residual spin-spin interaction in the system [7,8].

A resonance very similar to the neutron resonance has also been observed in Raman scattering experiments in the A_{1g} symmetry channel [9–13]. In YBCO the A_{1g} Raman resonance is located at 41 meV at optimal doping, and follows the neutron resonance energy with nickel and zinc substitutions [14,15]. This resonance is not seen in the B_{1g} symmetry, which is scanning the antinodal region of the Fermi surface, nor in the

B_{2g} channel, which is scanning the nodal region. In the B_{1g} channel, a SC coherence peak is observed at higher energy than the A_{1g} resonance. Its energy matches well twice the maximum of the d-wave SC gap $2\Delta_{SC}^0$ observed in other spectroscopies.

The A_{1g} Raman resonance has initially been attributed to the $2\Delta_{SC}^0$ SC pairing gap. However, later considerations showed that long-range Coulomb screening washes out the single-particle pair-breaking contribution to the Raman response in the A_{1g} channel leaving the position and the intensity of the A_{1g} Raman resonance essentially unexplained [16–19]. A two-magnon process has been proposed to explain the A_{1g} Raman resonance [18]. However, this process produces a resonance at twice the energy of the neutron resonance and thus cannot explain the near perfect energy matching between the A_{1g} Raman resonance and the Neutron resonance around the optimal doping.

From a theoretical point of view there are several open questions regarding the Raman resonance in the A_{1g} channel: Since the A_{1g} symmetry scans the whole Brillouin zone (BZ), how can we explain the absence of a superconducting coherent peak in the A_{1g} channel whereas it is observed in the B_{1g} channel? How can we explain that the A_{1g} resonance emerges at lower energy than the SC coherent peak one? How can we explain the perfect match between the energy of the Raman resonance in the A_{1g} channel and the INS frequency resonance at optimal doping? What is the information that this A_{1g} Raman resonance could give us about the physics of cuprates?

In this paper, we present a coherent scenario that provides an answer to the latter questions. Our scenario builds on recent experimental developments [20–30] that pinpointed the existence of a charge density wave (CDW) state, with ordering vector $\mathbf{q_c} = (q_x,0)$ and $\mathbf{q_c} = (0,q_y)$ with $q_x = q_y \approx 0.3\pi$ which exists between hole doping $p \approx 0.1$ until $p \approx 0.19$ [31] (see Fig. 1; note that the end point of the CDW order is still under debate). We explain the Raman resonance in the A_{1g} symmetry as a collective mode that allows excitations between the d-wave SC pairing sector and the observed d-wave CDW charge sector. The proposed scenario is supported by the fact

[*]xavier.montiel@cea.fr

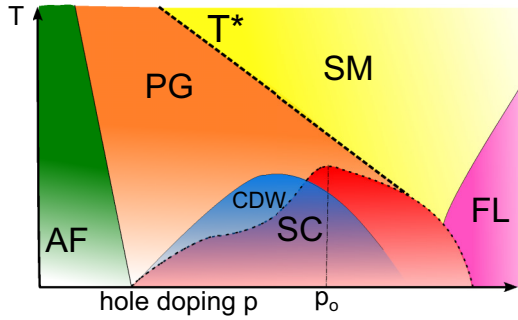[†]thomas.kloss@cea.fr

[‡]catherine.pepin@cea.fr

FIG. 1. Schematic temperature–hole doping (T, p) phase diagram of superconducting cuprates. At low hole doping, the system exhibits a Mott-insulator antiferromagnetic phase (AF). With increasing doping, d-wave superconductivity (SC) develops below the critical temperature T_c (dotted line). The maximum of critical temperature T_c is obtained at the optimal doping $p = p_o$. In the underdoped regime $p < p_o$, the pseudogap (PG) phase appears below the critical temperature $T^\star$ (dashed line). Above $T^\star$, cuprate compounds exhibit a metallic phase with a linear temperature dependence of the resistivity called strange metal (SM). In the overdoped regime $p > p_o$, T_c decreases and $T^\star$ meets T_c. Note that this behavior is true in the Bi2212 compound only. In other compounds, the behavior of the $T^\star$ line can be different. At very high doping, the system recovers a conventional Fermi liquid (FL) state. The charge density wave (CDW) order appears in the underdoped regime below $T^\star$ and above T_c (blue area). The hole doping where the CDW state disappears is still debated and thus we do not finish the transition line.

that the A_{1g} Raman resonance exists between $p = 0.12$ and $p = 0.22$ [32] which overlaps with the hole-doping range where a coexistence between a d-wave SC and a d-wave CDW ordered state have been observed [31] (see Fig. 1). This collective mode is a spin singlet $(S = 0)$ excitation with a charge ± 2 and we call it an η mode of the system.

In order to explain the A_{1g} Raman resonance, we assume the coexistence between a d-wave SC phase and a d-wave CDW ordered phase. The CDW phase has the same ordering vector as the observed one $\mathbf{q_c} = (q_x, 0)$ and $\mathbf{q_c} = (0, q_y)$ with $q_x = q_y \approx 0.3\pi$. This coexisting phase has been observed with STM in the Bi2212 compound [31].

A study of the Raman response in a coexistent d-wave SC and d-wave CDW order through an effective t-J model qualitatively explains the doping dependence of the frequency of the A_{1g} Raman resonance in the underdoped phase [33,34]. However, the authors considered a charge-ordering wave vector $\mathbf{Q} = (\pi, \pi)$, which is not observed experimentally, and the results did not reproduce the peak in the B_{1g} symmetry.

Here, we argue that the A_{1g} Raman resonance is the collective mode describing the proximity of the charge and pairing channels. Fluctuations between those two sectors are typically described by nonlinear σ models [35,36]. Within a model of itinerant electrons interacting through an effective AF spin-spin coupling, we find that the η resonance forms a particle-particle bound state situated below the $2\Delta_{SC}^0$ threshold, in a very similar way to the triplet spin exciton revealed by neutron scattering [7].

The paper is organized as follows: In Sec. II, we present the theoretical model we use to reproduce the experimental Raman data. We explain how we describe the different

phases of the cuprates (Sec. II A). We present the different susceptibilities that we consider (Sec. II B) and give details about the evaluation of the different Feynman diagrams (Sec. II C). We also explain the calculations of the full Raman response (Sec. II D). In Sec. III, we present the results of our theory and we compare them to the experimental data before concluding (Sec. IV). Explanations and information about the spin-fermion model and the experimental setup are given in detail in Appendices A and B, respectively.

II. THEORETICAL MODEL

A global explanation of the phase diagram of cuprate compounds is still lacking. For example, we still do not know whether the cuprates are fundamentally doped Mott insulators admitting a Coulomb energy repulsion of 1 eV which is crucial to explain the emergence of superconductivity (see, e.g., [37–39]), or whether an itinerant electron picture with strong antiferromagnetic (AF) fluctuations is a good approximation to explain the main features of the phase diagram (e.g., [40–42]). A consensus exists in the recognition that three main players are present in the phase diagram: d-wave superconductivity, AF order and fluctuations, and Mott-insulating phase. Note that the charge order could be a fourth key player of the cuprate compounds physics.

Below T^*, the PG phase critical temperature [43–45] (see Fig. 1), the influence of charge orderings seems to be stronger than previously thought [46]. On the theoretical point of view, the proximity between pairing and charge channel is well described by the spin-fermion approach. Such approach has been used through simplified eight hot spots (EHS) models in order to explain the PG phase [36,47]. In the framework of these models, the PG phase has been interpreted as a phase with a composite d-wave SC and d-wave bond order parameter related by SU(2) symmetry [36]. Note that the SU(2) symmetry relating the charge and spin channels is only realized in a strict sense in the eight hot spots model where the electronic dispersion has been linearized around each hot spot.

However, the CDW and PG phases are different phases as the CDW phase appears on the tips of the Fermi arcs after the antinodal zone has been gaped out (see Fig. 1). The study of SC and CDW competing orders related by angular fluctuations was performed in a model based on Landau theory [35]. In this model, the SU(2) symmetry can be recovered by ignoring the quartic and anisotropic couplings. Note that a spin-fermion approach was developed to explain the stability of the CDW phase related to modulated SC order called the pair density wave (PDW) [48]. In the following, we leave aside the complexity of the spin-fermion approach and we describe the SC/CDW coexisting phases with another model.

A. Description of the system

1. The two-body Hamiltonian

We consider a system of itinerant fermions interacting through an effective AF spin-spin coupling close to vector $\mathbf{Q}$ derived from the spin-fermion approach [36] (detailed in Appendix A). We then describe a system of fermions with a kinetic energy and nearest-neighbor interaction Hamiltonian

involving both spin and charge in the weak-coupling regime. The Hamiltonian is written $H = \sum_{i,j,\sigma} t_{ij} c_{i\sigma}^{\dagger} c_{j\sigma} + \sum_{\langle i,j \rangle} (J_{ij} \mathbf{S}_i \cdot \mathbf{S}_j + V_{ij} n_i n_j)$ where $n_i = \sum_{\sigma} c_{i\sigma}^{\dagger} c_{i\sigma}$ and $\mathbf{S}_i = \sum_{\alpha\beta} c_{i\alpha}^{\dagger} \sigma_{\alpha,\beta} c_{i\beta}$ are the density and spin operators, respectively, with $\sigma_{\alpha\beta}$ the Pauli matrix vector. $\langle ij \rangle$ denotes summation over nearest neighbors and t_{ij} is the hopping parameter. J_{ij} is the nearest-neighbor superexchange coupling and V_{ij} the nearest-neighbor Coulomb term. Long-range Coulomb effects will be considered later while discussing the Raman response. We will neglect them for the study of the collective mode. Involving the Fourier transform $c_{i,\sigma} = \frac{1}{\sqrt{N}} \sum_{\mathbf{k}} e^{i\mathbf{k}\cdot\mathbf{r}_i} c_{\mathbf{k},\sigma}$, where N is the total number of lattice sites, the Hamiltonian is written

$$
H = \sum_{\mathbf{k},\sigma} \xi_{\mathbf{k}} c_{\mathbf{k}\sigma}^{\dagger} c_{\mathbf{k}\sigma} + \sum_{\mathbf{k},\mathbf{k}',\mathbf{q}} (J_{\mathbf{q}} c_{\mathbf{k},\alpha}^{\dagger} \sigma_{\alpha\beta}^{T} c_{\mathbf{k}+\mathbf{q},\beta} c_{\mathbf{k}'+\mathbf{q},\gamma}^{\dagger} \sigma_{\gamma\delta} c_{\mathbf{k}',\delta})
$$

$$
+ \sum_{\mathbf{k},\mathbf{k}',\sigma,\sigma'} V_{\mathbf{q}} c_{\mathbf{k},\sigma}^{\dagger} c_{\mathbf{k}+\mathbf{q},\sigma} c_{\mathbf{k}',\sigma'}^{\dagger} c_{\mathbf{k}'-\mathbf{q},\sigma'}, \tag{1}
$$

where $c_{\mathbf{p},\alpha}^{(\dagger)}$ is the annihilation (creation) operator of an electron with spin α and impulsion $\mathbf{p}$. $\xi_{\mathbf{k}}$ is the one-particle energy with a tight-binding form obtained to fit ARPES data [49]: $\xi_{\mathbf{k}} = -2t[\cos(k_x a) + \cos(k_y a)] + 4t'\cos(k_x a)\cos(k_y a) + t_0[\cos(k_x a) - \cos(k_y a)]^2 - \mu$ where t, t' are respectively the first and second neighbor hopping terms with $t' = -0.3t$ and $t_0 = 0.084t$, which are third and fourth neighbor hopping terms. a is the cell parameter set to unity and μ is the chemical potential determined to adjust the hole doping. $J_{\mathbf{q}} = -\frac{J}{2}[\cos(q_x a) + \cos(q_y a)]$ is the Fourier transform of J_{ij} developed around $\mathbf{Q}$, while $V_{\mathbf{q}} = \frac{V}{2}[\cos(q_x a) + \cos(q_y a)]$ denotes the amplitude of the nearest-neighbor Coulomb interaction for small values of $\mathbf{q}$. $V_{\mathbf{q}}$ accounts for repulsion between charge and vanishes in the conventional t-J model. In the following, we treat $V_{\mathbf{q}}$ and $J_{\mathbf{q}}$ as independent parameters [5,50].

2. Order parameters and effective Hamiltonian

In the following, we focus on the superconducting phase where the Raman A_{1g} resonance peak has been observed. We consider that the superconducting phase around optimal doping is a coexistence between a d-wave SC order and the d-wave CDW order. Thus, we decouple the Hamiltonian (1) in the SC pairing channel and in the charge channel by introducing the two order parameters $\Delta_{\mathrm{SC},\mathbf{k}}$ and $\Delta_{\mathrm{CDW},\mathbf{k}}$. $\Delta_{\mathrm{SC},\mathbf{k}}$ is the superconducting order parameter which describes the d-wave SC order. $\Delta_{\mathrm{CDW},\mathbf{k}}$ is the CDW order parameter which describes the d-wave charge order with ordering vector $\mathbf{q_c}$. Applying the Hubbard-Stratonovitch transformation to the Hamiltonian (1), the effective Hamiltonian of the system can be written in the basis $\Psi_{\mathbf{k}}^{\dagger} = (c_{\mathbf{k},\sigma}^{\dagger}, c_{-\mathbf{k}-\mathbf{q_c},\bar{\sigma}}, c_{\mathbf{k}+\mathbf{q_c},\sigma}^{\dagger}, c_{-\mathbf{k},\bar{\sigma}})$ as

$$
\hat{G}^{-1}(\mathbf{k},\omega) = \begin{pmatrix} i\omega - \xi_{\mathbf{k}} & 0 & \Delta_{\mathrm{CDW},\mathbf{k}} & \Delta_{\mathrm{SC},\mathbf{k}} \\ 0 & i\omega + \xi_{-\mathbf{k}-\mathbf{q_c}} & \Delta_{\mathrm{SC},\mathbf{k}+\mathbf{q_c}}^{\dagger} & -\Delta_{\mathrm{CDW},\mathbf{k}} \\ \Delta_{\mathrm{CDW},\mathbf{k}}^{\dagger} & \Delta_{\mathrm{SC},\mathbf{k}+\mathbf{q_c}} & i\omega - \xi_{\mathbf{k}+\mathbf{q_c}} & 0 \\ \Delta_{\mathrm{SC},\mathbf{k}}^{\dagger} & -\Delta_{\mathrm{CDW},\mathbf{k}}^{\dagger} & 0 & i\omega + \xi_{-\mathbf{k}} \end{pmatrix} \tag{2}
$$

with $\xi_{-\mathbf{k}} = \xi_{\mathbf{k}}$. Note that the Green's function inverse matrix is very similar to previous studies with d-wave SC and d-wave CDW coexisting phase [33,34]. From inverting the matrix (2), one can find the Green's functions of the system. Particularly, the CDW quasiparticle Green's function $G^{\Delta_{\mathrm{CDW}}}(\mathbf{k},\omega)$ and the anomalous SC Green's function $G^{\Delta_{\mathrm{SC}}}(\mathbf{k},\omega)$ are written

$$
G^{\Delta_{\mathrm{CDW}}}(\mathbf{k},\omega) = \Delta_{\mathrm{CDW},\mathbf{k}} \frac{\Delta_{\mathrm{SC},\mathbf{k}+\mathbf{q_c}}^{\dagger} \Delta_{\mathrm{SC},\mathbf{k}} + |\Delta_{\mathrm{CDW},\mathbf{k}}|^2 - \xi_{\mathbf{k}+\mathbf{q_c}}\xi_{\mathbf{k}} + \omega^2 - i\omega(\xi_{\mathbf{k}+\mathbf{q_c}} + \xi_{\mathbf{k}})}{\det[\hat{G}(\mathbf{k},\omega)]}, \tag{3}
$$

$$
G^{\Delta_{\mathrm{SC}}}(\mathbf{k},\omega) = \frac{(\omega^2 + \xi_{\mathbf{k}+\mathbf{q_c}}^2 + |\Delta_{\mathrm{SC},\mathbf{k}+\mathbf{q_c}}|^2)\Delta_{\mathrm{SC},\mathbf{k}} + \Delta_{\mathrm{SC},\mathbf{k}+\mathbf{q_c}}|\Delta_{\mathrm{CDW},\mathbf{k}}|^2}{\det[\hat{G}(\mathbf{k},\omega)]}, \tag{4}
$$

with

$$
\det[\hat{G}^{-1}(\mathbf{k},\omega)] = |\Delta_{\mathrm{CDW},\mathbf{k}}|^4 + 2|\Delta_{\mathrm{CDW},\mathbf{k}}|^2 (\Delta_{\mathrm{SC},\mathbf{k}}\Delta_{\mathrm{SC},\mathbf{k}+\mathbf{q_c}} + \omega^2 - \xi_{\mathbf{k}+\mathbf{q_c}}\xi_{\mathbf{k}})
$$

$$
+ (\omega^2 + \xi_{\mathbf{k}}^2 + |\Delta_{\mathrm{SC},\mathbf{k}}|^2)(\omega^2 + \xi_{\mathbf{k}+\mathbf{q_c}}^2 + |\Delta_{\mathrm{SC},\mathbf{k}+\mathbf{q_c}}|^2). \tag{5}
$$

The Green's functions of the system will be crucial to estimate the different susceptibilities of the system (see Sec. II B).

3. Phenomenology and symmetries of the SC and CDW orders

In principle, we have to solve the self-consistent equations to determine $\Delta_{\mathrm{SC}}(k,\omega)$ and $\Delta_{\mathrm{CDW}}(k,\omega)$. However, the goal of this paper is not to explain the (T,p) phase diagram. Based on experimental evidence that the charge is modulated inside the superconducting phase of cuprates [31], we assume that the SC phase is composed of a competition between a d-wave SC phase and a d-wave CDW order. The amplitude of the order parameters $\Delta_{\mathrm{SC},\mathbf{k}}$ and $\Delta_{\mathrm{CDW},\mathbf{k}}$ is expected to vary with the hole doping. The CDW order has the same ordering wave vector $\mathbf{q_c}$ as the one observed experimentally. In this paper, we do not address the problem of the PG state. We then neglect the PG energy scale and we assume that the PG state does not interfere with the Raman response in the SC state. This assumption is expected to be valid around optimal doping and in the overdoped regime.

In Bi2212, the SC order parameter decreases above optimal doping $p = 0.16$ and vanishes around doping $p = 0.25$ as mentioned in [31]. The CDW order is maximal at doping $p = 0.12$ and vanishes around $p = 0.19$ at zero temperature [31], while the PG transition line meets the superconducting transition line at a slightly higher doping, around $p = 0.22$ [30,51].

We assume a simple momentum and frequency dependence of the SC pairing $\Delta_{SC}(k,\omega) = \frac{\Delta^0_{SC}}{2}[\cos(k_x a) - \cos(k_y a)]f(\omega, \Delta^0_{SC})$ and CDW order $\Delta_{CDW}(k,\omega) = \frac{\Delta^0_{CDW}}{2}[\cos(k_x a) - \cos(k_y a)]f(\omega, \Delta^0_{CDW})$ where Δ^0_{CDW} (Δ^0_{SC}) is the maximum of the d-wave CDW (SC) order and $f(\omega, X) = e^{-\frac{\omega^2}{2\sigma^2}}$ with a variance $\sigma = X/1.177$ ensuring a half width at half maximum equal to X. Recent STM experiments demonstrate the d-wave character of the CDW order [52].

Above optimal doping, the phase diagram (Fig. 1) shows that the superconducting state disappears at a higher temperature than the CDW state and we can consider that the CDW gap amplitude is lower than the SC one: $\Delta^0_{SC} > \Delta^0_{CDW}$. In the underdoped regime, the decreasing of T_c which goes below the CDW critical temperature (see Fig. 1) can be described by the opposite regime $\Delta^0_{SC} \leqslant \Delta^0_{CDW}$.

The frequency dependence of the order parameters is a consequence of the spin-fermion model [36,53]. We choose a frequency dependence of the order parameters that is a good approximation of the one coming from the spin-fermion model (see Appendix A).

4. SU(2) symmetry between SC and CDW order

The concept of emerging symmetries has first been introduced to explain PG phase of cuprate compounds. Particularly, a representation with a pseudospin operator was introduced which rotates the d-wave SC state into a charge order with ordering vector $q_c = (\pi, \pi)$ [54,55]. In systems with coexisting d-wave SC and CDW states, one can define a pseudospin respecting the SU(2) symmetry which rotates from the SC state onto a CDW order [56]. Indeed, in d-wave SC and CDW coexisting orders, we can define a pseudospin where each components is a SC or CDW operator with $\Delta_0 = \Delta_{CDW}$, $\Delta_1 = \Delta^\dagger_{SC}$, and $\Delta_{-1} = -\Delta^\dagger_1$,

$$\Delta_1 = -\frac{1}{\sqrt{2}} \sum_{\mathbf{k}} d_{\mathbf{k}} c^\dagger_{\mathbf{k}\uparrow} c^\dagger_{-\mathbf{k}\downarrow}, \qquad (6a)$$

$$\Delta_0 = \frac{1}{2} \sum_{\mathbf{k},\sigma} d_{\mathbf{k}} c^\dagger_{\mathbf{k}\sigma} c_{\mathbf{k}+\mathbf{q_c}\sigma}, \qquad (6b)$$

$$\Delta_{-1} = \frac{1}{\sqrt{2}} \sum_{\mathbf{k}} d_{\mathbf{k}} c_{\mathbf{k}\downarrow} c_{-\mathbf{k}\uparrow}, \qquad (6c)$$

with $d_{\mathbf{k}} = \frac{1}{2}[\cos(k_x a) - \cos(k_y a)]$ the d-wave form factor. The lowering and raising pseudospin operators η^+, $\eta^- = (\eta^+)^\dagger$, and η_z follow the definition

$$\eta^+ = \sum_{\mathbf{k}} c^\dagger_{\mathbf{k}\uparrow} c^\dagger_{-\mathbf{k}+\mathbf{q_c}\downarrow}, \qquad (7a)$$

$$\eta_z = \sum_{\mathbf{k}} \left(c^\dagger_{\mathbf{k}\uparrow} c_{\mathbf{k}\uparrow} + c^\dagger_{\mathbf{k}+\mathbf{q_c}\downarrow} c_{\mathbf{k}+\mathbf{q_c}\downarrow} - 1 \right). \qquad (7b)$$

The operators (7) form an SU(2) Lie algebra. The SU(2) spin operators (7) rotate each component of the pseudospin (6) into another [56].

A typical approach to study this underlying SU(2) symmetry is nonlinear σ models [35,36]. Such models have been proposed to explain the physics of cuprate superconductors [35,36,47,48]. In the following, we calculate the response of the operators η^+ and η^- that connect SC and CDW orders.

B. Susceptibilities of the system

1. The collective modes

In order to study the collective mode physics, we analyze the linear response for the two following operators. First, the INS resonance originates the excitation from the SC singlet state to the spin triplet at wave vector $\mathbf{Q}$ associated with the AF order [7]. It is described by the operator S_+ ($S_- = S^\dagger_+$):

$$S_+ = N^{-1/2} \sum_{\mathbf{k}} c^\dagger_{\mathbf{k}\uparrow} c_{\mathbf{k}+\mathbf{Q}\downarrow}, \qquad (8)$$

which destroy a bosonic excitation at momentum $\mathbf{Q}$ with a 0 charge and spin 1 as presented in Fig. 2(d). The η mode excites from the SC order parameter $\langle c^\dagger_{\mathbf{k}\uparrow} c^\dagger_{-\mathbf{k}\downarrow} \rangle$ to the CDW order $\langle c^\dagger_{\mathbf{k}\uparrow} c_{\mathbf{k}+\mathbf{q_c}\uparrow} \rangle$. It is described by the operator

$$\eta = N^{-1/2} \sum_{\mathbf{k}} c_{\mathbf{k}+\mathbf{q_c}\uparrow} c_{-\mathbf{k}\downarrow}, \qquad (9)$$

where $\mathbf{q_c}$ is the ordering vector of the charge density wave (CDW) order. The η operator destroy a bosonic excitation at momentum $\mathbf{q_c}$ with a 0 spin, a -2 charge, and is fully symmetric as presented in Fig. 2(e). Upon action of it, the SC state transforms into the CDW state in the same way as the operators (7a). The η mode is obtained at wave vector $\mathbf{q_c}$ with $\mathbf{q_c} = (0,q_y) = (q_x,0)$ and $q_x = q_y = 0.3\pi$, contrasting with the typical $\mathbf{Q} = (\pi,\pi)$ location of the spin triplet exciton. Within the framework of the eight hot spots spin-fermion model, where the electronic dispersion has been linearized
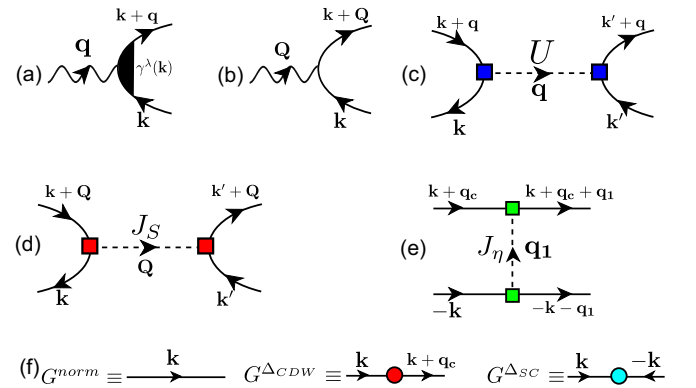

FIG. 2. Graphical representation for (a) the photon-electron vertex at $\mathbf{q}$ and for the symmetry λ and (b) the neutron-spin vertex at $\mathbf{Q} = (\pi,\pi)$. Graphical representation for (c) the Coulombian interaction vertex [17], (d) the spin triplet exciton vertex, and (e) the η-mode vertex. In (f) are presented the diagrammatic representation of the normal Green's functions, the CDW Green's function, and the SC anomalous Green's function.
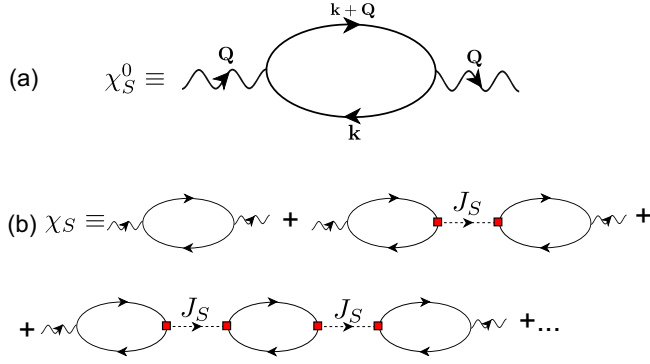
FIG. 3. (a) The bare polarization bubble we use for the spin mode. For the spin mode, the external momentum equals the AF ordering wave vector $\mathbf{Q} = (\pi, \pi)$. (b) Series of Feynman diagrams of the spin mode resulting from the RPA approximation. The spin susceptibility χ_S is the result of this series of diagrams which can be evaluated with the formula (10).

around the Fermi points, the operator described in Eq. (9) represents an SU(2) rotation between the CDW and SC states.

2. Susceptibilities in the random phase approximation and Bethe-Salpeter approximation

We rewrite the Hamiltonian (1) with the spin operators [$S_\pm$ of Eq. (8)] and the η-mode operator [see Eq. (9)] $H = \sum_{\mathbf{k},\sigma} \xi_{\mathbf{k}} c_{\mathbf{k}\sigma}^\dagger c_{\mathbf{k}\sigma} + J_S S_+ S_- + J_\eta \eta^\dagger \eta$. The magnitude of the interactions is $J_\eta = 3J - V$ in the η-mode channel and $J_S = 2J$ in the spin channel. We compare the spin susceptibility derived from the random phase approximation (RPA) with $\chi_S = -i\theta(t)\langle[S_+(t), S_-(0)]\rangle$ as depicted in Fig. 3 and the η-mode susceptibility derived from Bethe-Salpeter ladder approximation with $\chi_\eta = -i\theta(t)\langle[\eta(t), \eta^\dagger(0)]\rangle$ shown in Fig. 4. Within the RPA and Bethe-Salpeter approximation, the full susceptibilities are given by

$$\chi_\eta^\lambda(\omega) = \frac{\chi_\eta^{\lambda,1}(\omega)}{1 - J_\eta \chi_\eta^0(\omega)}, \quad \chi_S(\omega) = \frac{\chi_S^0(\omega)}{1 + J_S \chi_S^0(\omega)}, \quad (10)$$

where χ_S^0 is the bare polarization bubble for the spin mode [see Fig. 3(a)], χ_η^0 is the single segment of the ladder diagrams describing η mode [see Fig. 5(a)], and $\chi_\eta^{\lambda,1}$ is the first term of the diagram series for the η mode [see Fig. 5(b)] in the λ symmetry. Note that the detailed calculation of the bare polarization bubble and diagrams is done in Sec. II C.

C. Evaluation of the diagrams

In this section, we focus on the diagram calculation presented in Fig. 3(a), for the bare polarization of the spin mode χ_S^0, in Fig. 5(a) for the single segment of the ladder diagrams describing the η-mode χ_η^0 and in Fig. 5(b) for the first term of the η-mode diagram series. The explicit internal and external momenta dependence of each diagram is explicitly presented in Figs. 3(a) and 5.

In order to include the frequency dependence of the order parameters in the diagram calculation, we develop the order parameters depending on the internal frequency standing inside the summation terms around the external frequency,
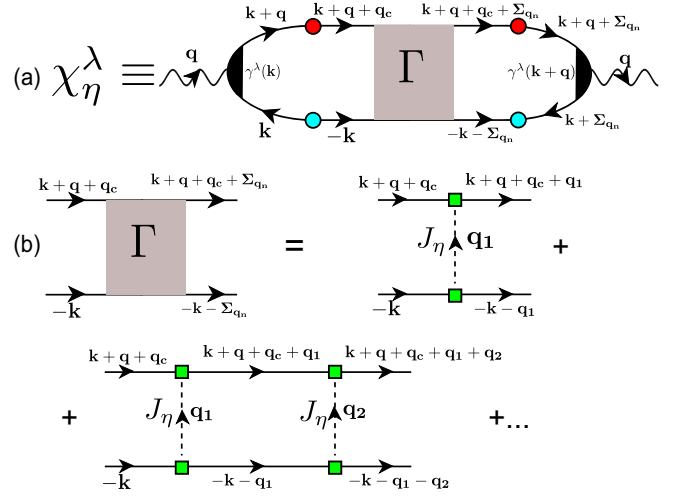

FIG. 4. (a) The Feynman diagram of the η collective mode. The red circle represents the CDW quasiparticle Green's functions $G^{\Delta_{\mathrm{CDW}}}$ of Eq. (3). The blue circle represents the anomalous SC function $G^{\Delta_{\mathrm{SC}}}$ of Eq. (4). $\gamma_{\mathbf{k}}^\lambda$ is the Raman vertex in the λ symmetry. (b) Γ is the diagram resulting from the Bethe-Salpeter series of diagrams. $\Sigma_n \mathbf{q_n}$ is the summation over the internal momenta $\mathbf{q_n}$. q_c is the charge density ware ordering vector. The value of the η collective mode susceptibility χ_η^λ is evaluated by the formula (10) in the approximation of a frequency- and momentum-independent J_η.

$\Delta(\varepsilon_{\mathrm{int}}) \approx \Delta(\varepsilon_{\mathrm{ext}}) + (\varepsilon_{\mathrm{int}} - \varepsilon_{\mathrm{ext}})\frac{\partial \Delta}{\partial \varepsilon_{\mathrm{int}}}\Big|_{\varepsilon_{\mathrm{int}}=\varepsilon_{\mathrm{ext}}} + \cdots$, and we keep only the zeroth-order term [with $\varepsilon_{\mathrm{int(ext)}}$ the internal (external) Matsubara frequency]. This implies that our susceptibility will be underestimated at high frequency.

We also assume that the η-mode interaction J_η and the spin interaction J_S do not depend on the frequency and the momentum. This approximation allows us to decompose the ladder diagram of Fig. 4 in the diagram of Fig. 5. The momentum sum is done over the first Brillouin zone with meshes of 400×400 after doing the summation over internal Matsubara frequencies at zero temperature $T = 0$. We do the analytical continuation on the external Matsubara frequency writing $i\omega \equiv \omega + i\delta$ in the energy denominators. A small broadening is introduced by the parameter δ and can be understood as a residual scattering.
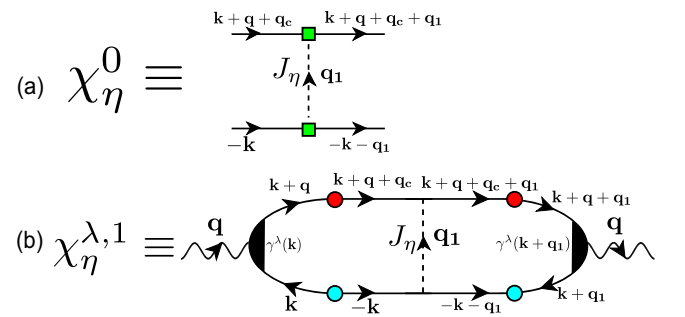

FIG. 5. (a) χ_η^0 is the single segment of the ladder diagrams describing the η mode. This term is evaluated in formula (12) in Sec. II C 1. (b) $\chi_\eta^{\lambda,1}$ is the first term of the series of ladder diagrams. $\gamma_{\mathbf{k}}^\lambda$ is the Raman vertex in the λ symmetry. This term is evaluated in formula (14) in Sec. II C 2. Both terms are evaluated in the approximation of a momentum- and frequency-independent J_η.
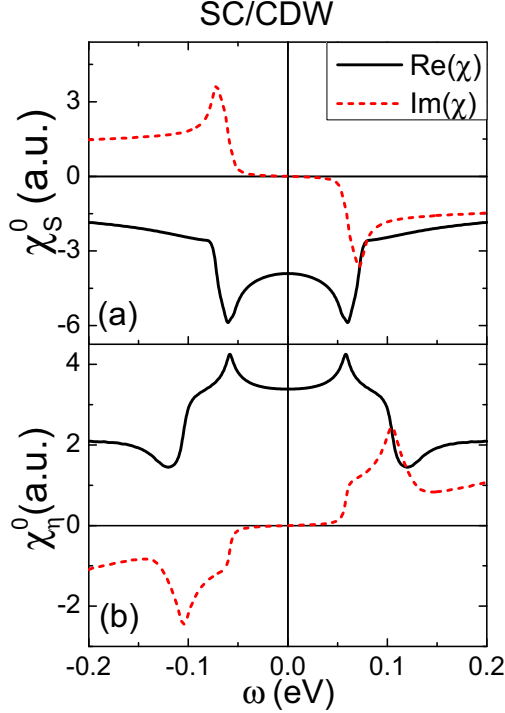
FIG. 6. Imaginary part (dashed line) and real part (solid line) of (a) the spin bare function χ_S^0 at $\mathbf{q} = \mathbf{Q} = (\pi,\pi)$ and (b) the η-mode bare function χ_η^0 at $\mathbf{q} = (0,0)$ at $T = 0$ K in a d-wave superconductor with $2\Delta_{SC}^0 = 60$ meV mixed with a d-wave charge order with $2\Delta_{CDW}^0 = 35$ meV. A broadening δ of 5 meV was employed.

1. Calculation of the bare polarization bubbles

The bare polarization χ^0 is the response function of the nonlocal density operator: $\chi^0 = -i\theta(\tau)\langle\rho_\mathbf{q}(\tau)\rho_\mathbf{q}(0)\rangle$ with $\rho_\mathbf{q} = 1/N \sum_\mathbf{k} c_\mathbf{k}^\dagger c_{\mathbf{k}+\mathbf{q}}$. From Fig. 3(a) and following the academic way to evaluate these diagrams, we find [50,57]

$$\chi_S^0(\mathbf{q},i\omega) = T \sum_{\varepsilon,\mathbf{k}} \text{Tr}[\hat{G}(i\varepsilon + i\omega, \mathbf{k}+\mathbf{q}) \cdot \hat{G}(i\varepsilon, \mathbf{k})], \quad (11)$$

where $\varepsilon(\omega)$ is a fermionic (bosonic) Matsubara frequency, T the temperature, and Tr means trace of the Green's function matrix $\hat{G}$ [see expression (2)]. $\hat{G}$ is the Green's function matrix deduced from the inversion of the matrix (2). From Fig. 5(a), and assuming that J_η is frequency and momenta independent, the ladder diagram χ_η^0 can be determined in the form [50,57]

$$\chi_\eta^0(\mathbf{k},\mathbf{q},\omega,\varepsilon) = T \sum_{\omega_1,\mathbf{q_1}} \text{Tr}[\hat{G}(i\varepsilon + i\omega + i\omega_1, \mathbf{k}+\mathbf{q}+\mathbf{q_1}+\mathbf{q_c})$$
$$\cdot \hat{G}(-i\varepsilon - i\omega_1, -\mathbf{k}-\mathbf{q_1})] \quad (12)$$

where ω_1 is a bosonic Matsubara frequency. Note that we put J_η outside of the expression (12). We do the internal Matsubara frequency and momentum summation by doing the change of variable $\tilde{\mathbf{k}} = \mathbf{k} + \mathbf{q_1}$ and $\tilde{\omega} = \omega_1 + \varepsilon$. Then, $\chi_\eta^0(\mathbf{k},\mathbf{q},\omega,\varepsilon)$ can
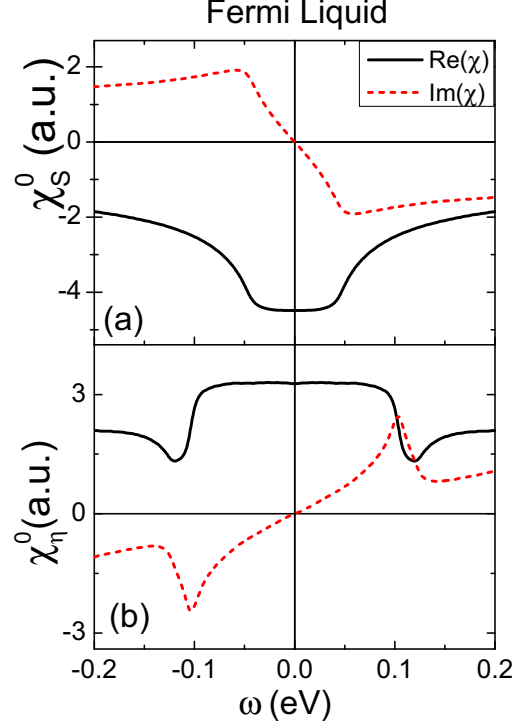

FIG. 7. Imaginary part (dashed line) and real part (solid line) of (a) the spin bare function χ_S^0 at $\mathbf{q} = \mathbf{Q} = (\pi,\pi)$ and (b) the η-mode bare function χ_η^0 at $\mathbf{q} = (0,0)$ at $T = 0$ K in the Fermi liquid phase. A broadening δ of 5 meV was employed.

be simplified as $\chi_\eta^0(\mathbf{q},i\omega)$ and becomes

$$\chi_\eta^0(\mathbf{q},\omega) = T \sum_{\tilde{\omega},\tilde{\mathbf{k}}} \text{Tr}[\hat{G}(i\tilde{\omega} + i\omega, \tilde{\mathbf{k}} + \mathbf{q} + \mathbf{q_c}) \cdot \hat{G}(-i\tilde{\omega}, -\tilde{\mathbf{k}})].$$
$$(13)$$

The bare polarization in the spin and η channels in the SC/CDW coexisting phase is presented in Fig. 6 (with $2\Delta_{SC}^0 = 63$ meV and $2\Delta_{CDW}^0 = 35$ meV) and in the Fermi liquid phase in Fig. 7. The bare polarization in the spin channel χ_S^0 develops a gap in the SC/CDW phase [Fig. 6(a)]. The presence of a threshold in Imχ_S^0 at the frequency $\omega \approx 60$ meV allows the emergence of a resonance of the collective response below the gap. This gap closes in the Fermi liquid phase as seen in Fig. 7(a).

On the other hand, the η mode couples an electron with momentum $\mathbf{k} + \mathbf{q_c}$ to a counterpropagating electron with momentum $-\mathbf{k}$. Consequently, χ_η^0 has an opposite sign of χ_S^0 in both Fermi liquid and superconducting state [see Fig. 6(b) and Fig. 7(d)]. In the η channel χ_η^0 develops a gap in the SC/CDW phase [Fig. 6(b)]. This quasiparticle gap closes in the Fermi liquid phase as seen in Fig. 7(b). We clearly see a gap with a threshold occurring around $\omega \approx 60$ meV which is the value of $2\Delta_{SC}^0$. Note that a gapped quasiparticle continuum develops at low frequency in χ_η^0 as in χ_S^0. The reason is that we evaluated χ_η^0 at $\mathbf{q} = \mathbf{0}$ while the CDW order has a nonzero ordering vector $\mathbf{q_c}$. For comparison, χ_S^0 is evaluated at finite momentum $\mathbf{q} = \mathbf{Q}$ which also results in a gapped quasiparticle continuum.

2. Calculation of the term $\chi_\eta^{\lambda,1}$

The ladder diagram $\chi_\eta^{\lambda,1}$ can be determined in the form [50,57]

$$\chi_\eta^{\lambda,1}(\mathbf{q},\omega) = -T^2 \sum_{\varepsilon,\omega_1,\mathbf{k},\mathbf{q_1}} J_\eta(\omega_1,\mathbf{q_1}) \gamma_{\mathbf{k}}^\lambda \gamma_{\mathbf{k+q+q_1}}^\lambda$$
$$\times [G^{\Delta_{\mathrm{CDW}}}(i\varepsilon + i\omega, \mathbf{k+q}) \cdot G^{\Delta_{\mathrm{SC}}}(i\varepsilon, \mathbf{k})$$
$$\times G^{\Delta_{\mathrm{CDW}}}(i\varepsilon + i\omega + i\omega_1, \mathbf{k+q+q_1+q_c})$$
$$\times G^{\Delta_{\mathrm{SC}}}(-i\varepsilon - i\omega_1, -\mathbf{k} - \mathbf{q_1})]. \quad (14)$$

Considering our initial approximation, we can factorize by the interaction J_η and we determine, from the Green's function matrix (2), that $G^{\Delta_{\mathrm{SC}}}(-i\varepsilon - i\omega_1, -\mathbf{k} - \mathbf{q_1}) = G^{\Delta_{\mathrm{SC}},\star}(i\varepsilon + i\omega_1, \mathbf{k+q_1})$ and $G^{\Delta_{\mathrm{CDW}}}(i\varepsilon + i\omega + i\omega_1, \mathbf{k+q+q_1+q_c}) = G^{\Delta_{\mathrm{CDW}},\star}(i\varepsilon + i\omega + i\omega_1, \mathbf{k+q+q_1})$. We do the internal Matsubara frequency and momentum summation by doing the change of variable $\tilde{\mathbf{k}} = \mathbf{k} + \mathbf{q_1}$ and $\tilde{\omega} = \omega_1 + \varepsilon$.

This susceptibility is proportional to the product of both SC and CDW order parameters $\Delta_{\mathrm{CDW}}\Delta_{\mathrm{SC}}$. Consequently, the η-mode susceptibility $\chi_\eta^{\lambda,1}$ only exists in a coexisting SC/CDW phase. A careful study of the symmetry of the η-mode response is done in the following section.

D. The full Raman response

We now argue that the η collective mode is seen in the A_{1g} Raman channel only. The study of the Raman susceptibility requires a careful examination of the symmetries of the system. These symmetries are taken into account by considering vertices in the photon-matter interaction different from unity (see Figs. 4 and 8). Three symmetries are typically considered for the Raman vertices in the cuprate superconductors which write within the effective mass approximation:

$$\gamma^{A_{1g}} = \frac{1}{2}\left[\frac{\partial^2 \xi_k}{\partial^2 k_x} + \frac{\partial^2 \xi_k}{\partial^2 k_y}\right], \quad \gamma^{B_{1g}} = \frac{1}{2}\left[\frac{\partial^2 \xi_k}{\partial^2 k_x} - \frac{\partial^2 \xi_k}{\partial^2 k_y}\right],$$
$$\gamma^{B_{2g}} = \frac{1}{2}\left[\frac{\partial^2 \xi_k}{\partial k_x \partial k_y} + \frac{\partial^2 \xi_k}{\partial k_y \partial k_x}\right],$$
$$(15)$$

where A_{1g} probes the whole Brillouin zone, B_{1g} the antinodal zone, and B_{2g} the nodal zone. Here we assume that there is no response in the A_{2g} symmetry [19] ($\gamma^{A_{2g}} = 0$). In the
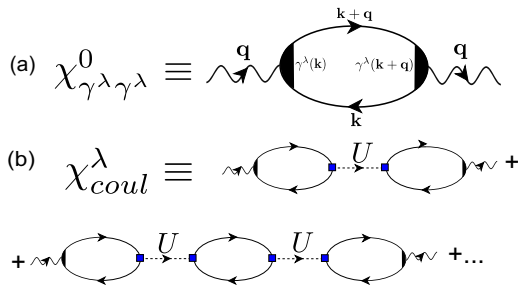

FIG. 8. (a) The Raman bare polarization bubble with γ^λ the Raman vertex in the λ symmetry. (b) $\chi_{\mathrm{coul}}^\lambda$ is the Coulomb screening term resulting from the RPA series of diagrams. Note that the dark triangle in the diagram denotes the presence of the Raman vertex.

presence of the η collective mode, the full Raman susceptibility is written in the λ symmetry

$$\chi_{\mathrm{Raman}}^\lambda = \chi_{\gamma^\lambda \gamma^\lambda}^0 + \chi_{\mathrm{coul}}^\lambda + \chi_\eta^\lambda, \quad (16)$$

where $\chi_{\gamma^\lambda \gamma^\lambda}^0$ is the bare Raman response [Fig. 8(a)], $\chi_{\mathrm{coul}}^\lambda$ the Coulomb screening [Fig. 8(b)], and χ_η^λ the η-mode response [Fig. 4(a)].

The value of χ_η^λ depends on the momentum dependence of the product $\gamma_{\mathbf{k}}^\lambda G^{\Delta_{\mathrm{CDW}}} G^{\Delta_{\mathrm{SC}}}$. The product of the two Green's functions $G^{\Delta_{\mathrm{CDW}}} G^{\Delta_{\mathrm{SC}}}$ is proportional to the product $\Delta_{\mathrm{SC}}\Delta_{\mathrm{CDW}}$ which is proportional to the square of the d-wave factor. The sum over the internal momenta in the first BZ of the square of the d-wave factor is finite. The sum over the internal momenta in the first BZ of the Raman vertex $\gamma_{\mathbf{k}}^{B_{1g}}$ and $\gamma_{\mathbf{k}}^{B_{2g}}$ vanishes ($\sum_k \gamma_k^{B_{1g}} = \sum_k \gamma_k^{B_{2g}} = 0$) while it is finite for the Raman vertex $\gamma_{\mathbf{k}}^{A_{1g}}$ ($\sum_k \gamma_k^{A_{1g}} \neq 0$). The sum over the internal momenta of the product $\gamma_{\mathbf{k}}^\lambda G^{\Delta_{\mathrm{CDW}}} G^{\Delta_{\mathrm{SC}}}$ therefore vanishes in the B_{1g} and B_{2g} symmetry while it is nonzero in the A_{1g} symmetry. Consequently, the η-mode response only exists in A_{1g} symmetry.

In addition long-range Coulomb interaction $U \sim 1/q^2$ plays an important role in screening the Raman in the A_{1g} channel [19]. Doing the summation over all the Coulomb diagram [Fig. 8(b)], one can find easily

$$\chi_{\mathrm{coul}}^\lambda = \frac{U \chi_{\gamma^\lambda 1}^0 \chi_{1\gamma^\lambda}^0}{1 - U \chi_{11}^0}, \quad (17)$$

where $\chi_{\gamma^\lambda 1}^0$ is the Raman susceptibility with one of the vertex put to unity and χ_{11}^0 the bare polarization bubble. In the limit $q \to 0$, the "Coulomb screened" susceptibility simplifies as $\chi_{\mathrm{coul}}^\lambda = -\chi_{\gamma^\lambda 1}^0 \chi_{1\gamma^\lambda}^0 / \chi_{11}^0$. In the A_{1g} symmetry, the contribution of $\chi_{\mathrm{coul}}^{A_{1g}}$ cannot be neglected [17]. Its contribution will screen partly the bare Raman susceptibility $\chi_{\gamma^{A_{1g}} \gamma^{A_{1g}}}^0$. Consequently, the Raman response in the A_{1g} symmetry is written $\chi_{\mathrm{Raman}}^{A_{1g}} = \chi_{\gamma^{A_{1g}} \gamma^{A_{1g}}}^0 + \chi_{\mathrm{coul}}^{A_{1g}} + \chi_\eta^{A_{1g}}$. Around optimal doping, we will see that the contribution of the η mode (last term) is of the same order of magnitude as the bare screened A_{1g} Raman response (first two terms). By increasing the doping, because of the weakening of the CDW order we expect a decrease of the η-mode intensity and the A_{1g} spectra will be dominated by the bare screened Raman response.

The Coulomb screening can be neglected in the B_{1g} and B_{2g} channels for symmetry reasons [17]. Consequently, the full Raman susceptibility is simply given by the unscreened response: $\chi_{\mathrm{Raman}}^\lambda \approx \chi_{\gamma^\lambda \gamma^\lambda}^0$ with $\lambda = B_{1g}$ (B_{2g}).

III. RESULTS AND DISCUSSION

The theoretical spectra are calculated without solving the self-consistent equation derived from the spin-fermion model. As a consequence, we need to adjust the amplitude of the order parameters as well as the value of J and V to reproduce the experimental data. The parameter values are adjusted in the following way: the value of Δ_{SC}^0 is chosen to reproduce the Raman peak frequency in the B_{1g} channel. The value of Δ_{CDW}^0 is chosen to adjust the intensity of the resonance in the A_{1g} channel. Note that the value of Δ_{CDW}^0 does not influence
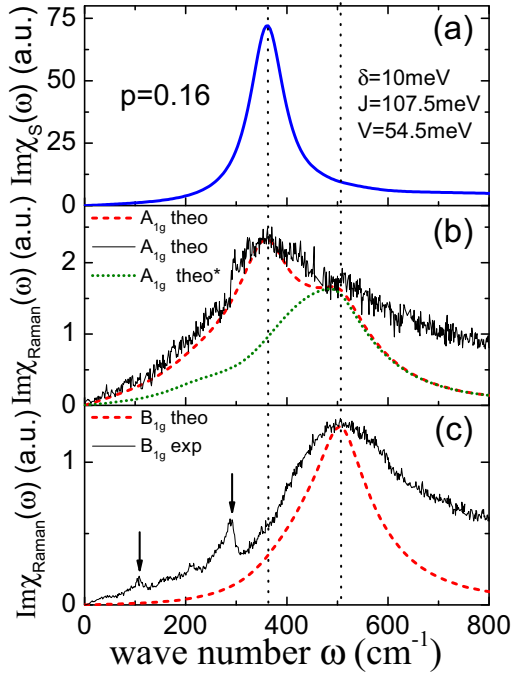
FIG. 9. (a) Calculated spin response. (b) Experimental (solid line) and calculated (dashed line) Raman response in the A_{1g} symmetry and (c) in the B_{1g} symmetry at optimal doping $p = 0.16$ ($\delta = 10$ meV, $2\Delta^0_{SC} = 63$ meV, $2\Delta^0_{CDW} = 45$ meV). In (b), the dotted line presents the calculated bare screened Raman response without the η-mode contribution, $\chi^{A_{1g}\star} = \chi^0_{\gamma^{A_{1g}}\gamma^{A_{1g}}} + \chi^{A_{1g}}_{coul}$. Phonon lines have been subtracted out of the experimental Raman spectra for clarity in (b) but not in (c). The arrows in (c) indicate the location of the phonon lines superimposed on the electronic background.

the frequency of the η mode. We adjust the value of J to fit the neutron resonance frequency and the value of V to fit the frequency of the Raman resonance in the A_{1g} symmetry. A fully self-consistent determination of the CDW and SC order parameter amplitude is not done here as our goal is to identify the main theoretical features necessary to explain the Raman resonance in the A_{1g} symmetry.

A. Results

The imaginary parts of the neutron spin susceptibility (spin response) and the full Raman susceptibility in the A_{1g} symmetry (Raman response) are presented in panels (a) and (b) of Fig. 9 for optimal doping ($p = 0.16$) with $2\Delta^0_{SC} = 63$ meV and $2\Delta^0_{CDW} = 45$ meV. The theoretical curves are obtained for $J = 107.5$ meV and $V = 54.5$ meV. To the best of our knowledge, the amplitude of the CDW order parameter Δ^0_{CDW} has not been evaluated yet in the experiments. However, in our effective model, the value of Δ^0_{CDW} is reasonable compared with the SC order parameter amplitude.

For this set of parameters, the calculated spin response exhibits a sharp peak at $\omega = 364$ cm^{-1} at the same energy as the energy of the calculated A_{1g} Raman resonance. Note that the frequency dependence of the CDW order Δ_{CDW} cuts the SC coherence peak at $2\Delta^0_{SC} \sim [510$ cm^{-1} (63 meV)] in the A_{1g} channel but leaves the B_{1g} channel unaffected [see panel (c)]. Figures 9(b) and 9(c) show a qualitative agreement between
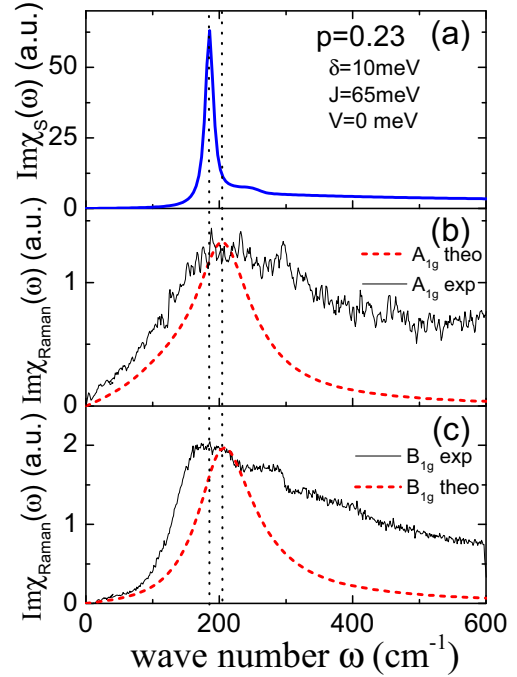
FIG. 10. (a) Calculated spin response. (b) Experimental (solid line) and calculated (dashed line) Raman response in the A_{1g} symmetry and (c) in the B_{1g} symmetry for the overdoped regime $p = 0.23$ ($\delta = 10$ meV, $2\Delta^0_{SC} = 25$ meV, $2\Delta^0_{CDW} = 0$ meV). Phonon lines have been subtracted out of the experimental A_{1g} Raman spectra in (b) for clarity.

the peak energies in the A_{1g} and B_{1g} calculated Raman spectra (red curves) and the experimental Raman spectra obtained from Bi2212 single crystals (black curves) [51]. We note that in our approximation, the calculated susceptibility vanishes in the metallic phase. This implies that we cannot reproduce the susceptibility at high energy for $\omega > 2\Delta^0_{SC}$. More realistic electron self-energies are needed in order to reproduce the spectra at high energy.

In the overdoped regime ($p = 0.23$), the value of $J = 65$ meV decreases and the value of V is the same as at optimal doping (see Fig. 10). Experimentally above optimal doping, the frequency of the INS resonance at **Q** decreases with overdoping and scales with T_c [4]. In the absence of experimental data, we choose to fit the neutron scattering peak by assuming that the scaling between the neutron resonance frequency and T_c observed by INS [4] is still valid at hole doping $p = 0.23$. At this doping, the INS resonance frequency should be at 187 cm^{-1} with $T_c = 50$ K. Note that persistent spin excitation has been observed in a huge range of hole doping by resonant inelastic x-ray scattering experiments [58,59], which favors the existence of neutron resonance at **Q** vector at high doping. The maximal value of Δ_{SC} and Δ_{CDW} weakens and we take into account this decreasing by putting $2\Delta^0_{SC} = 25$ meV and $2\Delta^0_{CDW} = 0$ meV. The decrease of Δ^0_{CDW} is due to the larger distance to the AF quantum critical point at this doping as well as the proximity of a change of Fermi surface topology [51,60]. The vanishing of the CDW order in the overdoped regime has been observed by STM [31].

For these parameters the calculated spin and A_{1g} Raman responses exhibit peaks at different energies (187 cm^{-1} and 205 cm^{-1}, respectively) [see Figs. 10(a) and 10(b)]. The perfect matching between neutron and raman peak energy is thus only verified close to optimal doping level. The theoretical Raman response captures well the energies of both the B_{1g} SC coherence peak $2\Delta_{SC}^0$ and the A_{1g} peak detected in the experimental spectra shown in Figs. 10(b) and 10(c).

The η mode also exists in the overdoped regime but the decreasing of Δ_{SC} and Δ_{CDW} completely weakens its intensity. The SC coherence peak, which is not detectable in the optimal doped regime [see Fig. 9(b)], increases its intensity with overdoping and becomes detectable in the A_{1g} channel around $p = 0.22$. Beyond this doping, the CDW order parameter amplitude vanishes and the η-mode contribution to the A_{1g} Raman spectrum vanishes. At this doping level the A_{1g} spectra are entirely given by the bare screened Raman response which peaks at a different energy than the neutron resonance. To summarize, the physical mechanism behind the A_{1g} resonance peak is different below $p = 0.22$ from what it is above. Below this doping, the A_{1g} resonance originates the η mode. Above this doping, the η mode vanishes with the CDW order and the peak in the A_{1g} channel is a 2Δ SC coherent peak located at the same energy as the one in the B_{1g} channel. This is qualitatively consistent with Raman experiments; more neutron data in the overdoped regime would be desirable to confirm this picture. Note that in Figs. 9 and 10, we adjust the units to superimpose the experimental and calculated data. Consequently, we cannot comment on the spectral weight of the results.

Before proceeding with the discussion, we briefly comment on the choice of parameters. In the AF state, *ab initio* calculations determine a superexchange coupling $J_{theo}^{AF} = 125$ meV [61–63]. An experimental value of superexchange coupling J_{AF}^{exp} has also been deduced from Raman scattering experiments in Bi2212 compounds and evaluated at $J \approx 125$ meV [64,65] in the AF phase. With hole doping, it is reasonable to assume that the superexchange coupling decreases $J < J_{AF}$ [65] because of the screening caused by the presence of holes. The values of J that we deduce from the fits (see Fig. 9 and Fig. 10) are comparable with the calculated and the experimental values, and are coherent with a decrease of the superexchange coupling with the hole doping. The value of V is weaker than the superexchange J. To the best of our knowledge, this value has not been evaluated yet. The nonzero value of the V parameter implies that the charge channel is important to explain the A_{1g} Raman resonance. The frequency of the A_{1g} Raman resonance depends on the values of V and J since it depends on $J_\eta = 3J - V$. Note that the A_{1g} Raman frequency is less sensitive to the value of V than to the value of J. Note that our effective model does not involve the strong correlation existing in the system. J and V have to be considered as effective parameters.

B. Discussion

In this part, we discuss our theoretical results and the main experimental features that characterize the Raman spectra in the A_{1g} and B_{1g} channels in the cuprates.

(1) The Raman experiments in the B_{1g} symmetry well established a long time ago the presence of the superconducting coherent peak at the frequency of twice the maximum of the d-wave SC gap $2\Delta_{SC}^0$ [9–13]. Note that the value of Δ_{SC}^0 can be determined by STM experiments [31]. Our theoretical model reproduces well this superconducting coherent peak for a large range of doping (see Figs. 9 and 10) [32].

(2) In Raman experiments at optimal doping, the Raman A_{1g} resonance appears at a frequency below the superconducting coherent peak frequency $2\Delta_{SC}^0$ [9–13] and at an energy very close to the INS resonance frequency at $\mathbf{Q} = (\pi, \pi)$ [14,15]. Our model explain this resonance by an η collective mode which rotates the SC ground state into a CDW state. The energy of this resonance depends on the interaction amplitude J and V as shown in Figs. 9(a) and 9(b). Although our model can reproduce the nearly identical energies of the A_{1g} Raman resonance and the neutron resonance, the equality is obtained by adjusting the parameter V. Nevertheless our model is able to reproduce this equality for a reasonable set of parameters

(3) In the overdoped regime, the Raman A_{1g} resonance is experimentally observed at an energy very close to the superconducting coherent peak frequency $2\Delta_{SC}^0$. In our calculations, the η collective mode vanishes in this regime because of the disappearance of the CDW order. Consequently, only the bare screened susceptibility contributes to the Raman response and the A_{1g} resonance becomes a superconducting coherence peak as shown in Figs. 10(a) and 10(b).

(4) In the underdoped regime, the transition temperature of the CDW order is greater than the superconducting critical temperature. Hence we can consider that the CDW order parameter amplitude becomes larger than the SC one $\Delta_{CDW}^0 > \Delta_{SC}^0$. In our theory this regime implies a decreasing of the η-mode resonance intensity which will become undetectable at low doping. Existing Raman data seem to be consistent with a disappearance of the A_{1g} in the underdoped regime [32]. The description of the underdoped regime however requires a description of the pseudogap phase that we did not take into account in the present work. Deeper considerations about the Raman scattering spectra in the underdoped regime will be considered in detail in a forthcoming work.

(5) To fit the Raman resonance in the A_{1g} symmetry, we propose an explanation based on the coexistence between two orders with a d-wave symmetry. This d-wave symmetry remains crucial to explain the resonance in the A_{1g} symmetry only. Moreover, the d-wave form factor of both SC and CDW orders has been observed with STM [52]. To explain the small amplitude of the 2Δ superconducting coherent peak in the A_{1g} symmetry, it is necessary to include a frequency dependence of the order parameters that can be predicted by the spin-fermion model. This frequency dependence suppresses the superconducting coherent peak from the η-mode response. In the bare Raman response, this superconducting coherent peak is strongly screened by the long-range Coulombian effects. This screening allows the observation of the η mode in this channel.

(6) Experimentally, the A_{1g} Raman resonance has been observed in the SC state and disappears at T_c [9–13]. The η mode calculated here depends on the magnitude of the CDW and SC order parameters and then we expect to see its disappearance for temperature below T_c in the overdoped part of the phase diagram (where $\Delta_{SC}^0 > \Delta_{CDW}^0$). This is a limitation of the approach developed here. However, we

argue that the η mode exists between SC order and all types of charge orders. In our simplified model, we neglect the contributions that could come from the PG phase. In the framework where the PG phase is interpreted as a charge order, one could observe the emergence of such η resonance at higher temperature than the CDW critical temperature [66].

IV. CONCLUSION

To conclude, we propose a coherent scenario to explain the resonance peak in the A_{1g} symmetry seen in Raman scattering. This scenario is based on the existence of coexisting d-wave SC and d-wave CDW orders in the SC phase of the cuprates. The ubiquitous proximity of the CDW and SC states in the underdoped phase of the cuprates generates a collective "η mode" allowing rotations between those two states. The η collective mode results from the coupling between the d-wave SC and the d-wave CDW state. This mode produces a response in Raman scattering spectroscopy solely in the A_{1g} symmetry and matches the spin triplet resonance at $\mathbf{q} = \mathbf{Q} = (\pi,\pi)$ at optimal doping. Since the η mode is a charge ± 2 spin-zero spin-singlet excitation other probes such as electron energy loss spectroscopy and resonant x-ray techniques are also likely to show the resonance.

APPENDIX A: SUPPLEMENTARY INFORMATION ABOUT THE SPIN-FERMION MODEL

In this section, we present the calculation of the effective Lagrangian derived from the initial spin-fermion Lagrangian. The goal of this section is to give more physical details for the completeness of the paper.

1. The spin-fermion model and the effective boson propagator

The starting point of the theoretical model is the spin-fermion model [36,47]. Note that the models presented in [36,47] simplify the Fermi surface (FS) in eight hot spots (EHS) [the hot spots are points of the Fermi surface separated by the vector $\mathbf{Q} = (\pi,\pi)$]. In the following, we develop the model introduced in [36] in the whole Brillouin zone (BZ).

In the model [36], the physics of cuprates results from the coupling of the fermions with a bosonic spin mode which generates at the antiferromagnetic (AF) / pseudogap (PG) quantum critical point (QCP) a pseudogap in the fermionic dispersion. This new state, different from the AF one, is a superposition of a d-wave superconducting (SC) state and a charge density wave (CDW) order. This bosonic spin mode

(also called paramagnons) survives out of the AF phase and become the new glue between electrons that leads to the PG and superconducting (SC) phase. To describe the interaction between this bosonic spin mode and fermions, we start from the Lagrangian $L = L_c + L_\phi$, where

$$L_c = c^*(\partial_\tau + \xi_k + \lambda\phi\sigma)c, \tag{A1}$$

$$L_\phi = \frac{1}{2}\phi\left[\frac{\omega^2}{v_s^2} + (\mathbf{q} - \mathbf{Q})^2 + m\right]\phi + \frac{u}{2}(\phi^2)^2. \tag{A2}$$

The Lagrangian L describes the coupling of the electron (represented by the fermionic field c) to spin waves (represented by the bosonic field ϕ). The dynamic of the fermions and their coupling with the bosonic mode is described in the Lagrangian L_c. The strength of this coupling is tuned by the parameter λ which couples c and ϕ. The fermionic dispersion is described by $\xi_k = \varepsilon_k - \mu$ where ε_k is the fermionic dispersion and μ the chemical potential and affords us a description of the Fermi surface of the system.

The bosonic spin mode physics is described in the Lagrangian L_ϕ. v_s is the velocity of the spin waves, ω is the bosonic Matsubara frequency, the paramagnon mass m describes the distance to the QCP ($m > 0$ in the metallic side and vanishes at the QCP), and $\mathbf{Q} = (\pi,\pi)$ is the ordering wave vector in the AF phase.

The spin-wave propagator $D_q^{-1} = [\frac{\omega^2}{v_s^2} + (\mathbf{q} - \mathbf{Q})^2 + m]$ is renormalized by the particle-hole bubble [36]. This renormalization leads us to consider the effective spin-wave propagator D_{eff} that is written $D_{\text{eff},k}^{-1} = (\gamma|\omega| + |\mathbf{k}|^2 + m)$ where γ is a phenomenological coupling constant and $\mathbf{k}$ has formally been shifted by $\mathbf{Q}$.

In the following, we simplify the notation as $k \equiv (i\omega,\mathbf{k})$, where $i\omega$ are fermionic Matsubara frequencies. To integrate out the bosonic degrees of freedom, we neglect the spin-wave interaction ($u = 0$). The partition function is then written

$$Z = \int d[\Psi]\exp(-S_0 - S_{\text{int}}), \tag{A3}$$

$$S_0 = \sum_{k,\sigma} \Psi_{k,\sigma}^\dagger G_{0,k,\sigma}^{-1} \Psi_{k,\sigma}, \tag{A4}$$

$$S_{\text{int}} = -\sum_{k,k',q,\sigma} J_q c_{k,\sigma}^\dagger c_{k+Q+q,\bar{\sigma}} c_{k',\bar{\sigma}}^\dagger c_{k'-q-Q,\sigma}^\dagger, \tag{A5}$$

where the bare propagator is

$$\hat{G}_{0k}^{-1} = \begin{pmatrix} i\omega - \xi_k & 0 & 0 & 0 \\ 0 & i\omega + \xi_{-k+q_c} & 0 & 0 \\ 0 & 0 & i\omega - \xi_{k-q_c} & 0 \\ 0 & 0 & 0 & i\omega + \xi_{-k} \end{pmatrix} \tag{A6}$$

and the spinor field $\Psi_k = (c_{k,\sigma}, c_{-k+q_c,\bar{\sigma}}^\dagger, c_{k-q_c,\sigma}, c_{-k,\bar{\sigma}}^\dagger)$. Moreover, $J_q^{-1} = 4D_q^{-1}/3\lambda^2$, $\sigma = \{\uparrow,\downarrow\}$ labels the spin, and $\mathbf{q_c}$ stands for the charge density wave ordering vector.

2. The mean-field decoupling and the effective Lagrangian

After the integration on the bosonic degrees of freedom, we decouple the two-body action S_{int} using mean-field

decoupling. Thus, we decouple the interaction Lagrangian in the SC channel and in the charge channel by introducing the two order parameters Δ_k and $\Delta_{\mathrm{CDW},k}$. Δ_k is the superconducting order parameter which describes the d-wave SC order. $\Delta_{\mathrm{CDW},k}$ is the CDW order parameter which describes the d-wave charge order with ordering vector $\mathbf{q_c}$. In the framework of the EHS model [36], these two order parameters are related to the SU(2) symmetry which is verified at the hot spot. The SU(2) symmetry between SC and CDW order exists if their energy level is the same (the energy splitting $\Delta_k - \Delta_{\mathrm{CDW},k}$ vanishes). In the whole Brillouin zone, the SU(2) symmetry is verified around the hot spots (at low paramagnon mass) and at the zone edge (at high paramagnon mass) [53].

Applying the Hubbard-Stratanovitch transformation to the interaction S_{int}, the partition function becomes

$$Z = \frac{\int d[\Psi] d[\Delta, \Delta_{\mathrm{CDW}}] \exp(-S_0 - S_{\mathrm{int,eff}})}{\int d[\Delta, \Delta_{\mathrm{CDW}}] \exp(-S_q)}, \quad \text{(A7)}$$

$$S_q = -\sum_{k,q,\sigma} \left[J_q^{-1} \Delta_{\mathrm{CDW},k}^\dagger \Delta_{\mathrm{CDW},\bar{k}+q} + J_q^{-1} \Delta_k^\dagger \Delta_{\bar{k}+q} \right], \quad \text{(A8)}$$

$$S_{\mathrm{int,eff}} = S_q - \sum_{k,\sigma} \Psi_{k,\sigma}^\dagger \hat{M}_k \Psi_{k,\sigma}, \quad \text{(A9)}$$

where $\bar{k} = k + Q$ and the matrix $\hat{M}_k$ is

$$\hat{M}_k = \begin{pmatrix} & \hat{m}_k \\ \hat{m}_k^\dagger & \end{pmatrix}, \quad \hat{m}_k = \begin{pmatrix} -\Delta_{\mathrm{CDW},k} & -\Delta_k \\ -\Delta_{k+q_c}^\dagger & \Delta_{\mathrm{CDW},-k} \end{pmatrix}. \quad \text{(A10)}$$

Finally, the effective Lagrangian we will use in the following will be defined as $\hat{G}^{-1} = \hat{G}_{0k}^{-1} - \hat{M}_k$. One can integrate over the fermionic degrees of freedom and find the mean-field equations [53]

$$\hat{M}_{\omega,\mathbf{k}} = T \sum_{\omega',\mathbf{k}'} J_{\mathbf{k}-\mathbf{k}'-\mathbf{Q}} \hat{G}_{\omega',\mathbf{k}'}. \quad \text{(A11)}$$

The matrix equation can be projected onto the different components. The exact solution of these equations goes beyond the goal of the paper. However, we directly see that the order parameters depend on the frequency as well as on the momentum.

3. Frequency dependence at the hot spot

The frequency dependence is a key player of the theory. Then we solve Eq. (A11) for the superconducting component $\Delta_{\omega,\mathbf{k}}$ only, putting the CDW order parameter to zero ($\Delta_{\omega,\mathbf{k}}^{\mathrm{CDW}} = 0$). Considering a temperature of $T = 0.001$ and a paramagnon
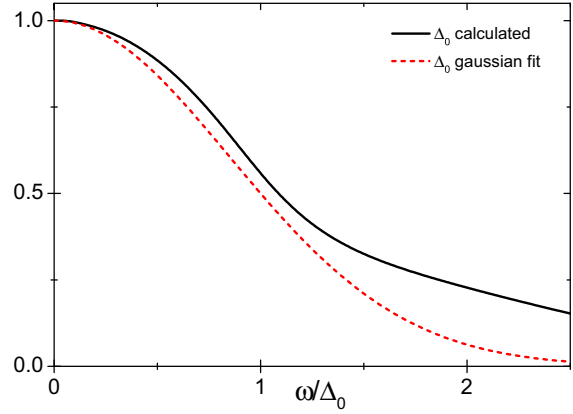

FIG. 11. The frequency dependence of the superconducting order parameter $\Delta_{\mathbf{k}}$ at the hot spot calculated from the mean-field equation (A11). The frequency form factor which is a Gaussian with a half-width of Δ_0 which is the value of the SC order parameter at zero frequency.

mass of $m = 10^{-6}$ with $\gamma = 10^{-5}$ and $\lambda = 12$, the frequency dependence of the SC order parameter at the hot spot is shown in Fig. 11.

As shown in Fig. 11, the Gaussian frequency form factor can reproduce the frequency dependence of the SC order parameter. In the main text, we assume that the frequency dependence of the CDW order parameter can be fitted by the same form factor. The calculation of the frequency dependence of the order parameters at each doping and each temperature is left for later work.

APPENDIX B: RAMAN EXPERIMENTS

Raman experiments were carried out using a triple-grating spectrometer (JY-T64000) equipped with a liquid-nitrogen-cooled CCD detector. The 532 nm laser excitation line was used from respectively a diode pump solid state laser. Measurements in the SC state were performed at 10 K using an ARS closed-cycle He cryostat. Raman study was performed on Bi2212 single crystals with two distinct levels of doping $p = 0.16$ ($T_c = 90$ K) and $p = 0.23$ ($T_c = 52$ K). The level of doping was controlled only by oxygen insertion [51]. The B_{1g} channel was obtained from crossed polarizations at 45° from the Cu-O bond direction. The A_{1g} channel was obtained from parallel polarizations along the Cu-O bond (given $A_{1g} + B_{1g}$) and normalized subtraction of the B_{1g} channel. All the spectra have been corrected for the Bose factor and the instrumental spectral response. They are thus proportional to the imaginary part of the Raman response function $\mathrm{Im}\,\chi_R^\lambda(\omega)$ ($\lambda = A_{1g}$ or B_{1g}).

[1] J. Rossat-Mignod, L. Regnault, C. Vettier, P. Bourges, P. Burlet, J. Bossy, J. Henry, and G. Lapertot, Physica C **185-189**, Part 1, 86 (1991).

[2] P. Bourges, B. Keimer, S. Pailhès, L. Regnault, Y. Sidis, and C. Ulrich, Physica C **424**, 45 (2005).

[3] V. Hinkov, S. Pailhes, P. Bourges, Y. Sidis, A. Ivanov, A. Kulakov, C. T. Lin, D. P. Chen,

C. Bernhard, and B. Keimer, Nature (London) **430**, 650 (2004).

[4] H. He, Y. Sidis, P. Bourges, G. D. Gu, A. Ivanov, N. Koshizuka, B. Liang, C. T. Lin, L. P. Regnault, E. Schoenherr, and B. Keimer, Phys. Rev. Lett. **86**, 1610 (2001).

[5] E. Demler and S.-C. Zhang, Phys. Rev. Lett. **75**, 4126 (1995).

[6] E. Demler, W. Hanke, and S.-C. Zhang, Rev. Mod. Phys. **76**, 909 (2004).

[7] O. Tchernyshyov, M. R. Norman, and A. V. Chubukov, Phys. Rev. B **63**, 144507 (2001).

[8] G. Stemmann, C. Pépin, and M. Lavagna, Phys. Rev. B **50**, 4075 (1994).

[9] S. L. Cooper, F. Slakey, M. V. Klein, J. P. Rice, E. D. Bukowski, and D. M. Ginsberg, Phys. Rev. B **38**, 11934 (1988).

[10] T. Staufer, R. Nemetschek, R. Hackl, P. Müller, and H. Veith, Phys. Rev. Lett. **68**, 1069 (1992).

[11] A. Sacuto, R. Combescot, N. Bontemps, P. Monod, V. Viallet, and D. Colson, Europhys. Lett. **39**, 207 (1997).

[12] Y. Gallais, A. Sacuto, and D. Colson, Physica C **408-410**, 785 (2004).

[13] M. Le Tacon, A. Sacuto, and D. Colson, Phys. Rev. B **71**, 100504 (2005).

[14] Y. Gallais, A. Sacuto, P. Bourges, Y. Sidis, A. Forget, and D. Colson, Phys. Rev. Lett. **88**, 177401 (2002).

[15] M. Le Tacon, Y. Gallais, A. Sacuto, and D. Colson, J. Phys. Chem. Solids **67**, 503 (2006).

[16] T. P. Devereaux and D. Einzel, Phys. Rev. B **51**, 16336 (1995).

[17] T. Strohm and M. Cardona, Phys. Rev. B **55**, 12725 (1997).

[18] F. Venturini, U. Michelucci, T. P. Devereaux, and A. P. Kampf, Phys. Rev. B **62**, 15204 (2000).

[19] T. P. Devereaux and R. Hackl, Rev. Mod. Phys. **79**, 175 (2007).

[20] J. E. Hoffman, E. W. Hudson, K. M. Lang, V. Madhavan, H. Eisaki, S. Uchida, and J. C. Davis, Science **295**, 466 (2002).

[21] T. Hanaguri, C. Lupien, Y. Kohsaka, D. H. Lee, M. Azuma, M. Takano, H. Takagi, and J. C. Davis, Nature (London) **430**, 1001 (2004).

[22] N. Doiron-Leyraud, C. Proust, D. LeBoeuf, J. Levallois, J.-B. Bonnemaison, R. Liang, D. A. Bonn, W. N. Hardy, and L. Taillefer, Nature (London) **447**, 565 (2007).

[23] S. E. Sebastian, N. Harrison, R. Liang, D. A. Bonn, W. N. Hardy, C. H. Mielke, and G. G. Lonzarich, Phys. Rev. Lett. **108**, 196403 (2012).

[24] N. Doiron-Leyraud, S. Lepault, O. Cyr-Choinière, B. Vignolle, G. Grissonnanche, F. Laliberté, J. Chang, N. Barišić, M. K. Chan, L. Ji, X. Zhao, Y. Li, M. Greven, C. Proust, and L. Taillefer, Phys. Rev. X **3**, 021019 (2013).

[25] W. D. Wise, M. C. Boyer, K. Chatterjee, T. Kondo, T. Takeuchi, H. Ikuta, Y. Wang, and E. W. Hudson, Nat. Phys. **4**, 696 (2008).

[26] M. Fujita, H. Hiraka, M. Matsuda, M. Matsuura, J. M. Tranquada, S. Wakimoto, G. Xu, and K. Yamada, J. Phys. Soc. Jpn. **81**, 011007 (2012).

[27] Y. He, Y. Yin, M. Zech, A. Soumyanarayanan, M. M. Yee, T. Williams, M. C. Boyer, K. Chatterjee, W. D. Wise, I. Zeljkovic, T. Kondo, T. Takeuchi, H. Ikuta, P. Mistark, R. S. Markiewicz, A. Bansil, S. Sachdev, E. W. Hudson, and J. E. Hoffman, Science **344**, 608 (2014).

[28] W. Tabis, Y. Li, M. Le Tacon, L. Braicovich, A. Kreyssig, M. Minola, G. Dellea, E. Weschke, M. J. Veit, M. Ramazanoglu, A. I. Goldman, T. Schmitt, G. Ghiringhelli, N. Barišić, M. K. Chan, C. J. Dorow, G. Yu, X. Zhao, B. Keimer, and M. Greven, Nat. Commun. **5**, 5875 (2014).

[29] S. Blanco-Canosa, A. Frano, E. Schierle, J. Porras, T. Loew, M. Minola, M. Bluschke, E. Weschke, B. Keimer, and M. Le Tacon, Phys. Rev. B **90**, 054513 (2014).

[30] I. M. Vishik, M. Hashimoto, R.-H. He, W.-S. Lee, F. Schmitt, D. Lu, R. G. Moore, C. Zhang, W. Meevasana, T. Sasagawa, S. Uchida, K. Fujita, S. Ishida, M. Ishikado, Y. Yoshida, H. Eisaki, Z. Hussain, T. P. Devereaux, and Z.-X. Shen, Proc. Natl. Acad. Sci. USA **109**, 18332 (2012).

[31] K. Fujita, C. K. Kim, I. Lee, J. Lee, M. Hamidian, I. A. Firmo, S. Mukhopadhyay, H. Eisaki, S. Uchida, M. J. Lawler, E. A. Kim, and J. C. Davis, Science **344**, 612 (2014).

[32] S. Benhabib, Y. Gallais, M. Cazayous, M.-A. Méasson, R. D. Zhong, J. Schneeloch, A. Forget, G. D. Gu, D. Colson, and A. Sacuto, Phys. Rev. B **92**, 134502 (2015).

[33] E. Cappelluti and R. Zeyher, Phys. Rev. B **59**, 6475 (1999).

[34] R. Zeyher and A. Greco, Phys. Rev. Lett. **89**, 177004 (2002).

[35] L. E. Hayward, D. G. Hawthorn, R. G. Melko, and S. Sachdev, Science **343**, 1336 (2014).

[36] K. B. Efetov, H. Meier, and C. Pépin, Nat. Phys. **9**, 442 (2013).

[37] P. A. Lee, N. Nagaosa, and X.-G. Wen, Rev. Mod. Phys. **78**, 17 (2006).

[38] E. Gull, O. Parcollet, and A. J. Millis, Phys. Rev. Lett. **110**, 216405 (2013).

[39] S. Sorella, G. B. Martins, F. Becca, C. Gazza, L. Capriotti, A. Parola, and E. Dagotto, Phys. Rev. Lett. **88**, 117002 (2002).

[40] A. Abanov, A. V. Chubukov, and J. Schmalian, Adv. Phys. **52**, 119 (2003).

[41] M. R. Norman and C. Pépin, Rep. Prog. Phys. **66**, 1547 (2003).

[42] A. Chubukov, D. Pines, and J. Schmalian, in *Superconductivity*, edited by K. Bennemann and J. Ketterson (Springer, Berlin, 2008).

[43] H. Alloul, T. Ohno, and P. Mendels, Phys. Rev. Lett. **63**, 1700 (1989).

[44] W. W. Warren, R. E. Walstedt, G. F. Brennert, R. J. Cava, R. Tycko, R. F. Bell, and G. Dabbagh, Phys. Rev. Lett. **62**, 1193 (1989).

[45] J. Tallon and J. Loram, Physica C **349**, 53 (2001).

[46] M. H. Hamidian, S. D. Edkins, K. Fujita, A. Kostin, A. P. Mackenzie, H. Eisaki, S. Uchida, M. J. Lawler, E.-A. Kim, S. Sachdev, and J. C. Séamus Davis, arXiv:1508.00620.

[47] M. A. Metlitski and S. Sachdev, Phys. Rev. B **82**, 075128 (2010).

[48] Y. Wang and A. Chubukov, Phys. Rev. B **90**, 035149 (2014).

[49] A. A. Kordyuk, S. V. Borisenko, M. Knupfer, and J. Fink, Phys. Rev. B **67**, 064504 (2003).

[50] J. R. Schrieffer, *Theory of Superconductivity* (Benjamin, Reading, MA, 1964).

[51] S. Benhabib, A. Sacuto, M. Civelli, I. Paul, M. Cazayous, Y. Gallais, M. A. Méasson, R. D. Zhong, J. Schneeloch, G. D. Gu, D. Colson, and A. Forget, Phys. Rev. Lett. **114**, 147001 (2015).

[52] M. H. Hamidian, S. D. Edkins, C. K. Kim, J. C. Davis, A. P. Mackenzie, H. Eisaki, S. Uchida, M. J. Lawler, E.-A. Kim, S. Sachdev, and K. Fujita, Nat. Phys. (2015).

[53] T. Kloss, X. Montiel, and C. Pépin, Phys. Rev. B **91**, 205124 (2015).

[54] C. N. Yang, Phys. Rev. Lett. **63**, 2144 (1989).

[55] C. N. Yang and S. C. Zhang, Mod. Phys. Lett. B **04**, 759 (1990).

[56] H.-Y. Kee, H. Doh, and T. Grzesiak, J. Phys.: Condens. Matter **20**, 255248 (2008).

[57] A. Abrikosov, L. P. Gor'kov, and I. Y. Dzyaloshinskii, *Quantum Field Theoretical Methods in Statistical Physics* (Pergamon Press, Oxford, 1965).

[58] M. Le Tacon, G. Ghiringhelli, J. Chaloupka, M. M. Sala, V. Hinkov, M. W. Haverkort, M. Minola, M. Bakr, K. J. Zhou, S. Blanco-Canosa, C. Monney, Y. T. Song, G. L. Sun, C. T. Lin, G. M. De Luca, M. Salluzzo, G. Khaliullin, T. Schmitt, L. Braicovich, and B. Keimer, Nat. Phys. **7**, 725 (2011).

[59] M. P. M. Dean, G. Dellea, R. S. Springell, F. Yakhou-Harris, K. Kummer, N. B. Brookes, X. Liu, Y.-J. Sun, J. Strle, T. Schmitt, L. Braicovich, G. Ghiringhelli, I. Bozovic, and J. P. Hill, Nat. Mater. **12**, 1019 (2013).

[60] A. Kaminski, S. Rosenkranz, H. M. Fretwell, M. R. Norman, M. Randeria, J. C. Campuzano, J.-M. Park, Z. Z. Li, and H. Raffy, Phys. Rev. B **73**, 174511 (2006).

[61] C. J. Calzado and J.-P. Malrieu, Phys. Rev. B **63**, 214520 (2001).

[62] D. Muñoz, I. de P. R. Moreira, and F. Illas, Phys. Rev. B **65**, 224521 (2002).

[63] A. E. Ruckenstein, P. J. Hirschfeld, and J. Appel, Phys. Rev. B **36**, 857 (1987).

[64] S. Sugai and M. Sato, Phys. Rev. B **40**, 9292 (1989).

[65] G. Blumberg, M. Kang, M. V. Klein, K. Kadowaki, and C. Kendziora, Science **278**, 1427 (1997).

[66] T. Kloss, X. Montiel, and C. Pépin, arXiv:1510.03038.